85. Yang, S.Q.; Lin, H.Z.; Lane, M.D.; Clemens, M.; Diehl, A.M. Obesity increases sensitivity to endotoxin liver injury: Implications for the pathogenesis of steatohepatitis. *Proc. Natl. Acad. Sci. USA* **1997**, *94*, 2557–2562.
86. Seki, E.; de Meicis, S.; Osterricher, C.H.; Kluwe, J.; Osawa, Y.; Brenner, D.A.; Schwabe, R.F. TLR4 enhances TGF-beta signaling and hepatic fibrosis. *Nat. Med.* **2007**, *13*, 1324–1332.
87. Jagavelu, K.; Routray, C.; Shergill, U.; O'Hara, S.P.; Faubion, W.; Shah, V.H. Endothelial cell toll-like receptor 4 regulates fibrosis-associated angiogenesis in the liver. *Hepatology* **2010**, *52*, 590–601.
88. Shirai, Y.; Yoshiji, H.; Noguchi, R.; Kaji, K.; Aihara, Y.; Douhara, A.; Moriya, K.; Namisaki, T.; Kawaratani, H.; Fukui, H. Cross talk between toll-like receptor-4 signaling and angiotensin-II in liver fibrosis development in the rat model of non-alcoholic steatohepatitis. *J. Gastroenterol. Hepatol.* **2013**, *28*, 723–730.
89. Henao-Mejia, J.; Elinav, E.; Jin, C.-C.; Hao, L.; Mehal, W.Z.; Strowig, T.; Thaiss, C.A.; Kau, A.L.; Eisenbarth, S.C.; Jurczak, M.J.; *et al.* Inflammasome-mediated dysbiosis regulates progression of NAFLD and obesity. *Nature* **2012**, *482*, 179–185.
90. Li, L.; Chen, L.; Hu, L.; Liu, Y.; Sun, H.Y.; Tang, Y.-J.; Chang, Y.-X.; Tu, Q.-Q.; Feng, G.-S.; Shen, F.; *et al.* Nuclear factor high-mobility group box1 mediating the activation of Toll-like receptor 4 signaling in hepatocytes in the early stage of nonalcoholic fatty liver disease in mice. *Hepatology* **2011**, *54*, 1620–1630.
91. Chen, A.; Tang, Y.; Davis, V.; Hsu, F.-F.; Kennedy, S.M.; Song, H.; Turk, J.; Brunt, E.M.; Newberry, E.P.; Davidson, N.O. Liver fatty acid binding protein (L-Fabp) modulates murine stellate cell activation and diet-induced nonalcoholic fatty liver disease. *Hepatology* **2013**, *57*, 2202–2212.
92. Ratziu, V.; Charlotte, F.; Bernhardt, C.; Giral, P.; Halbron, M.; Lenaour, G.; Hartmann-Heurtier, A.; Bruckert, E.; Poynard, T.; LIDO Study Group. Long-term efficacy of rosiglitazone in nonalcoholic steatohepatitis: Results of the fatty liver improvement by rosiglitazone therapy (FLIRT 2) extension trial. *Hepatology* **2010**, *51*, 445–453.
93. Miura, K.; Yang, L.; van Rooijen, N.; Ohnishi, H.; Seki, E. Hepatic recruitment of macrophages promotes nonalcoholic steatohepatitis through CCR2. *Am. J. Physiol. Gastrointest. Liver Physiol.* **2012**, *302*, G1310–G1321.
94. Tosello-Trampont, A.-C.; Landes, S.G.; Nguyen, V.; Novobrantseva, T.I.; Hahn, Y.S. Kupffer cells trigger nonalcoholic steatohepatitis development in diet-induced mouse model through tumor necrosis factor-α production. *J. Biol. Chem.* **2012**, *287*, 40161–40172.
95. Carpino, G.; Renzi, A.; Onori, P.; Gaudio, E. Role of hepatic progenitor cells in nonalcoholic fatty liver disease development: Cellular cross-talks and molecular networks. *Int. J. Mol. Sci.* **2013**, *14*, 20112–20130.
96. Van Hul, N.K.M.; Abarca-Quinones, J.; Sempoux, C.; Horsmans, Y.; Leclercq, I.A. Relation between liver progenitor cell expansion and extracellular matrix deposition in a CDE-induced murine model of chronic liver injury. *Hepatology* **2009**, *49*, 1625–1635.
97. Boulter, L.; Govaere, O.; Bird, T.G.; Radulescu, S.; Ramachandran, P.; Pellicoro, A.; Ridgway, R.A.; Seo, S.S.; Spee, B.; Rooijen, N.V.; *et al.* Macrophage derived Wnt signaling opposes Notch

signaling in a Numb mediated manner to specify HPC fate in chronic liver disease in human and mouse. *Nat. Med.* **2012**, *18*, 572–579.

98. Nobili, V.; Carpino, G.; Alisi, A.; Franchitto, A.; Alpini, G.; de Vito, R.; Onori, P.; Alvaro, D.; Gaudio, E. Hepatic progenitor cells activation, fibrosis, and adipokines production in pediatric nonalcoholic fatty liver disease. *Hepatology* **2012**, *56*, 2142–2153.
99. Friedman, S.L. Convergent pathways that cause hepatic fibrosis in NASH. *Nat. Rev. Gastroenterol. Hepatol.* **2013**, *10*, 71–72.
100. Wagner, M.; Zollner, G.; Trauner, M. Nuclear receptors in liver disease. *Hepatology* **2011**, *53*, 1023–1034.
101. Belfort, R.; Harrison, S.A.; Brown, K.; Darland, C.; Finch, J.; Hardies, J.; Balas, B.; Gastaldeli, A.; Tio, F.; Pulcini, J.; *et al.* A placebo-controlled trial of pioglitazone in subjects with nonalcoholic steatohepatitis. *N. Eng. J. Med.* **2006**, *355*, 2297–2307.
102. Syn, W.-K.; Choi, S.S.; Liaskou, E.; Karaca, G.F.; Agboola, K.M.; Oo, Y.H.; Mi, Z.; Pereira, T.A.; Zdanowicz, M.; Malladi, P.; *et al.* Osteopontin is induced by hedgehog pathway activation and promotes fibrosis progression in nonalcoholic steatohepatitis. *Hepatology* **2011**, *53*, 106–115.
103. Okazaki, I.; Watanabe, T.; Hozawa, S.; Niioka, M.; Arai, M.; Maruyama, K. Minireview Series for the 50th Volume: Reversibility of hepatic fibrosis: From the first report of collagenase in the liver to the possibility of gene therapy for recovery. *Keio J. Med.* **2001**, *50*, 58–65.
104. Arthur, M.J.; Friedman, S.L.; Roll, F.J.; Bissell, D.M. Lipocytes from normal rat liver release a neutral metalloproteinase that degrades basement membrane (type IV collagen). *J. Clin. Invest.* **1989**, *84*, 1076–1085.
105. Takahara, T.; Furui, K.; Funaki, J.; Nakayama, Y.; Itoh, H.; Miyabayashi, C.; Sato, H.; Seiki, M.; Ooshima, A.; Watanabe, A. Increased expression of matrix metalloproteinase-II in experimental liver fibrosis in rats. *Hepatology* **1995**, *21*, 787–795.
106. Takahara, T.; Furui, K.; Yata, Y.; Jin, B.; Zhang, L.P.; Nambu, S.; Sato, H.; Seiki, M.; Watanabe, A. Dual expression of matrix metalloproteinase-2 and membrane-type-1-matrix metalloproteinase in fibrotic human livers. *Hepatology* **1997**, *26*, 1521–1529.
107. Okazaki, I.; Nabeshima, K. Introduction: MMPs, ADAMs/ADAMTSs research products to achieve big dream. *Anticancer Agents Med. Chem.* **2012**, *12*, 688–706.
108. Iredale, J.P.; Benyon, R.C.; Pickering, J.; McCullen, M.; Northrop, M.; Pawley, S.; Hovell, C.; Arthur, M.J. Mechanism of spontaneous resolution of rat liver fibrosis. Hepatic stellate cell apoptosis and reduced hepatic expression of metalloproteinase inhibitors. *J. Clin. Invest.* **1998**, *102*, 538–549.
109. Yoshiji, H.; Kuriyama, S.; Yoshii, J.; Ikenaga, Y.; Noguchi, R.; Nakatani, T.; Tsujinoue, H.; Yanase, K.; Namisaki, T.; Imazu, H.; *et al.* Tissue inhibitor of metalloproteinase-1 attenuates spontaneous liver fibrosis resolution in the transgenic mouse. *Hepatology* **2002**, *36*, 850–860.
110. Ljumovic, D.; Diamantis, I.; Alegakis, A.K.; Kouroumalis, E.A. Differential expression of matrix metalloproteinases in viral and non-viral chronic liver diseases. *Clin. Chim. Acta* **2004**, *349*, 203–211.
111. D'Amico, F.; Consolo, M.; Amoroso, A.; Skarmoutsou, E.; Mauceri, B.; Stivala, F.; Malaponte, G.; Bertino, G.; Neri, S.; Mazzarino, M.C. Liver immunolocalization and plasma levels of MMP-9

in non-alcoholic steatohepatitis (NASH) and hepatitis C infection. *Acta Histochem.* **2010**, *112*, 474–481.

112. Cao, Q.; Mak, K.; Lieber, C.S. Leptin represses matrix metalloproteinase-1 gene expression in LX2 human hepatic stellate cells. *J. Hepatol.* **2007**, *46*, 124–133.
113. Wanninger, J.; Walter, R.; Bauer, S.; Eisinger, K.; Schaffler, A.; Dorn, C.; Weiss, T.S.; Hellerbrand, C.; Buechler, C. MMP-9 activity is increased by adiponectin in primary human hepatocytes but even negatively correlates with serum adiponectin in a rodent model of non-alcoholic steatohepatitis. *Exp. Mol. Pathol.* **2011**, *91*, 603–607.
114. Tarrats, N.; Moles, A.; Garcia-Ruiz, C.; Fernandez-Checa, J.C.; Mari, M. Critical role of tumor necrosis factor receptor 1, but not 2, in hepatic stellate cell proliferation, extracellular matrix remodeling, and liver fibrogenesis. *Hepatology* **2011**, *54*, 319–327.
115. Adams, L.A.; Lymp, J.F.; St. Sauver, J.; Sanderson, S.O.; Lindor, K.D.; Feldstein, A.; Angulo, P. The natural history of nonalcoholic fatty liver disease: A population-based cohort study. *Gastroenterology* **2005**, *129*, 113–121.
116. Ascha, M.S.; Hanouneh, I.A.; Lopez, R.; Tamimi, T.A.-R.; Feldstein, A.F.; Zein, N.N. The incidence and risk factors of hepatocellular carcinoma in patients with nonalcoholic steatohepatitis. *Hepatology* **2010**, *51*, 1972–1978.
117. Fu, J.; Chen, Y.; Cao, J.; Luo, T.; Qian, Y.; Yang, W.; Ren, Y.; Su, B.; Cao, G.; Yang, Y.; *et al.* P28 GANK overexpression accelerates hepatocellular carcinoma invasiveness and metastasis via phosphoinositol 3-kinae/AKT/hypoxia-inducible factor-1α pathways. *Hepatology* **2011**, *53*, 181–192.
118. Hayashi, Y.; Osanai, M.; Lee, G.H. Fascin-1 expression correlates with repression of E-cadherin expression in hepatocellular carcinoma cells and augments their invasiveness in combination with matrix metalloproteinases. *Cancer Sci.* **2011**, *102*, 1226–1235.
119. Wang, B.; Hsu, S.; Majumder, S.; Kutay, H.; Huang, W.; Jacob, S.T.; Ghoshal, K. TGFbeta-mediated upregulation of hepatic miR-181b promotes hepatocarcinogenesis by targeting TIMP3. *Oncogene* **2010**, *29*, 1787–1797.
120. Man, K.; Ng, K.T.P.; Xu, A.; Cheng, Q.; Lo, C.M.; Xiao, J.W.; Sun, B.S.; Lim, Z.X.H.; Cheung, J.S.; Wu, E.X.; *et al.* Suppression of tumor growth and metastasis by adiponectin in nude mice through inhibition of tumor angiogenesis and downregulation of Rho kinase/IFN-inducible protein 10/matrix metalloproteinase 9 signaling. *Clin. Cancer Res.* **2010**, *16*, 967–977.
121. Gentilini, A.; Rombouts, K.; Galastri, S.; Caligiuri, A.; Mingarelli, E.; Mello, T.; Marra, F.; Mantero, S.; Roncalli, M.; Invernizzi, P.; *et al.* Role of the stromal-derived factor-1 (SDF-1)-CXCR4 axis in the interaction between hepatic stellate cells and cholangiocarcinoma. *J. Hepatol.* **2012**, *57*, 813–820.
122. Marrero, J.A.; Fontana, R.J.; Su, G.L.; Conjeevaram, H.S.; Emick, D.M.; Lok, A.S. NAFLD may be a common underlying liver disease in patients with hepatocellular carcinoma in the United States. *Hepatology* **2002**, *36*, 1349–1354.
123. Ratziu, V.; Bonyhay, L.; di Charlotte, F.; Cavallaro, L.; Sayegh-Tainturier, M.H.; Giral, P.; Grimaldi, A.; Opolon, P.; Poynard, T. Survival, liver failure and hepatocellular carcinoma in obesity-related cryptogenic cirrhosis. *Hepatology* **2002**, *35*, 1485–1493.

124. Paradis, V.; Zalinski, S.; Chelbi, E.; Guedj, N.; Degos, F.; Vilgrain, V.; Bedossa, P.; Belghiti, J. Hepatocellular carcinomas in patients with metabolic syndrome often develop without significant liver fibrosis: A pathological analysis. *Hepatology* **2009**, *49*, 851–859.
125. Zhang, D.Y.; Friedman, S.L. Fibrosis-dependent mechanism of hepatocarcinogenesis. *Hepatology* **2012**, *56*, 769–775.
126. Yin, C.; Evason, K.J.; Asahina, K.; Stainer, D.Y.R. Hepatic stellate cells in liver development, regeneration, and cancer. *J. Clin. Invest.* **2013**, *123*, 1902–1910.
127. Muir, K.; Hazim, A.; He, Y.; Peyressatre, M.; Kim, D.-Y.; Song, X.; Beretta, L. Proteomic and lipidomic signatures of lipid metabolism in NASH-associated hepatocellular carcinoma. *Cancer Res.* **2013**, *73*, 4722–4731.
128. Page, J.M.; Harrison, S.A. NASH and HCC. *Clin. Liver Dis.* **2009**, *13*, 631–647.
129. Bohinc, B.N.; Diehl, A.M. Mechanism of disease progression in NASH: New paradigms. *Clin. Liver Dis.* **2012**, *16*, 549–565.
130. Weiskopf, K.; Ring, A.M.; Ho, C.C.M.; Volkmer, J.-P.; Levin, A.M.; Volkmer, A.K.; Özkan, E.; Fernhoff, N.B.; van de Rijn, M.; Weissman, I.L.; *et al.* Engineered SIRPα variants as immunotherapeutic adjuvants to anti-cancer antibodies. *Science* **2013**, *341*, 88–91.
131. Yoshimoto, S.; Loo, T.M.; Atarashi, K.; Kanda, H.; Sato, S.; Oyadomari, S.; Iwakura, Y.; Oshima, K.; Morita, H.; Hattori, M.; *et al.* Obesity-induced gut microbial metabolite promotes liver cancer through senescence secretome. *Nature* **2013**, *499*, 97–101.
132. Lin, H.; Yan, J.; Wang, Z.; Hua, F.; Yu, J.; Sun, W.; Li, K.; Liu, H.; Yang, H.; Lv, Q.; *et al.* Loss of immunity-supported senescence enhances susceptibility to hepatocellular carcinogenesis and progression in Toll-like receptor 2-deficient mice. *Hepatology* **2013**, *57*, 171–182.
133. Wang, Z.; Yan, J.; Lin, H.; Hua, F.; Wang, X.; Liu, H.; Lv, X.; Yu, J.; Mi, S.; Wang, J.; *et al.* Toll-like receptor 4 activity protects against hepatocellular tumorigenesis and progression by regulating expression of DNA repair protein Ku70 in mice. *Hepatology* **2013**, *57*, 1869–1881.
134. Murphy, S.K.; Yang, H.; Moylan, C.A.; Pang, H.; Dellinger, A.; Abdelmalek, M.F.; Garrett, M.; Ashley-Koch, A.; Suzuki, A.; Tillmann, H.L.; *et al.* Relationship between methylome and transcriptome in patients with nonalcoholic fatty liver disease. *Gastroenterology* **2013**, *145*, 1076–1087.
135. Arii, S.; Mise, M.; Harada, T.; Furutani, M.; Ishigami, S.; Niwano, M.; Mizumoto, M.; Fukumoto, M.; Imamura, M. Overexpression of matrix metalloproteinase 9 gene in hepatocellular carcinoma with invasive potential. *Hepatology* **1996**, *24*, 316–322.
136. Ashida, K.; Nakatsukasa, H.; Higashi, T.; Ohguchi, S.; Hino, N.; Nouso, K.; Urabe, Y.; Yoshida, K.; Kinugasa, N.; Tsuji, T. Cellular distribution of 92-kd type IV collagenase B in human hepatocellular carcinoma. *Am. J. Pathol.* **1996**, *149*, 1803–1811.
137. Ogata, R.; Torimura, T.; Kin, M.; Ueno, T.; Tateishi, Y.; Kuromatsu, R.; Shimauchi, Y.; Sakamoto, M.; Tamaki, S.; Sata, M.; *et al.* Increased expression of membrane type 1 matrix metalloproteinases and matrix metalloproteinase-2 with tumor differentiation in hepatocellular carcinomas. *Hum. Pathol.* **1999**, *30*, 443–450.
138. Sakamoto, Y.; Mafune, K.; Mori, M.; Shiraishi, T.; Imamura, H.; Mori, M.; Takayama, T.; Makuuchi, M. Overexpression of MMP-9 correlates with growth of small hepatocellular carcinoma. *Int. J. Oncol.* **2000**, *17*, 237–243.

139. Maatta, M.; Soini, Y.; Liakka, A.; Autio-Harmainen, H. Differential expression of matrix metalloproteinase (MMP)-2, MMP-9, and membrane type 1-MMP in hepatocellular and pancreatic adenocarcinoma: Implications for tumor progression and clinical prognosis. *Clin. Cancer Res.* **2000**, *6*, 2726–2734.
140. Syed, I.; Rathod, J.; Parmar, M.; Parmar, M.; Corcoran, G.B.; Ray, S.D. Matrix metalloproteinase-9, -10, and -12, MDM2 and p53 expression in mouse liver during diethylnitrosamine-induced oxidative stress and genomic injury. *Mol. Cell Biochem.* **2012**, *365*, 351–361.
141. Fang, J.-H.; Zhou, H.-C.; Zeng, C.; Yang, J.; Liu, Y.; Huang, X.; Zhang, J.-P.; Guan, X.-Y.; Zhuang, S.-M. MicroRNA-29b suppresses tumor angiogenesis, invasion, and metastasis by regulating matrix metalloproteinase 2 expression. *Hepatology* **2011**, *54*, 1729–1740.
142. Sato, H.; Takino, T.; Okada, Y.; Cao, J.; Shinagawa, A.; Yamamoto, E.; Seiki, M. A matrix metalloproteinase expressed on the surface of invasive tumor cells. *Nature* **1994**, *370*, 61–65.
143. Strongin, A.Y.; Collier, I.; Bannikov, G.; Marmer, B.L.; Grant, G.A.; Goldberg, G.L. Mechanism of cell surface activation of 72-kDa type IV collagenase. Isolation of the activated form of the membrane metalloproteinase. *J. Biol. Chem.* **1995**, *270*, 5331–5338.
144. Yamamoto, H.; Itoh, F.; Adachi, Y.; Sakamoto, H.; Adachi, M.; Hinoda, Y.; Imai, K. Relation of enhanced secretion of active matrix metalloproteinases with tumor spread in human hepatocellular carcinoma. *Gastroenterology* **1997**, *112*, 1290–1296.
145. Musso, O.; Theret, N.; Campion, J.P.; Turlin, B.; Milani, S.; Grappone, C.; Clement, B. *In situ* detection of matrix metalloproteinase-2 (MMP2) and the metalloproteinase inhibitor TIMP2 transcripts in human primary hepatocellular carcinoma and in liver metastasis. *J. Hepatol.* **1997**, *26*, 593–605.
146. Harada, T.; Arii, S.; Imamura, T.; Higashitsuji, H.; Furutani, M.; Niwano, M.; Ishigami, S.; Fukumoto, M.; Seiki, M.; Sato, H.; *et al.* Membrane-type matrix metalloproteinase-1 (MT1-MMP) gene is overexpressed in highly invasive hepatocellular carcinoma. *J. Hepatol.* **1998**, *28*, 231–239.
147. Theret, N.; Musso, O.; L'Helgoualc'h, A.; Campion, J.-P.; Clement, B. Differential expression and origin of membrane-type 1 and 2 matrix metalloproteinases (MT-MMPs) in association with MMP2 activation in injured human livers. *Am. J. Pathol.* **1998**, *153*, 945–954.
148. Yamamoto, H.; Itoh, F.; Adachi, Y.; Fukushima, H.; Itoh, H.; Sasaki, S.; Hinoda, Y.; Imai, K. Messenger RNA expression of matrix metalloproteinases and tissue inhibitors of metalloproteinases in human hepatocellular carcinoma. *Jpn. J. Clin. Oncol.* **1999**, *29*, 58–62.
149. McKenna, G.J.; Chen, Y.; Smith, R.M.; Meneghetti, A.; Ong, C.; McMaster, R.; Scudamore, C.H.; Chung, S.W. A role for matrix metalloproteinases and tumor host interaction in hepatocellular carcinomas. *Am. J. Surg.* **2002**, *183*, 588–594.
150. Giannelli, G.; Bergamini, C.; Marinosci, F.; Fransvea, E.; Quaranta, M.; Lupo, L.; Schiraldi, O.; Antonaci, S. Clinical role of MMP-2/TIMP-2 imbalance in hepatocellular carcinoma. *Int. J. Cancer* **2002**, *97*, 425–431.
151. Ishii, Y.; Nakasato, Y.; Kobayashi, S.; Yamazaki, Y.; Aoki, T. A study on angiogenesis-related marix metalloproteinase networks in primary hepatocellular carcinoma. *J. Exp. Clin. Cancer Res.* **2003**, *22*, 461–470.

152. Gao, Z.H.; Tretiakova, M.S.; Liu, W.H.; Gong, C.; Farris, P.D.; Hart, J. Association of E-cadherin, matrix metalloproteinases, and tissue inhibitors of metalloproteinases with the progression and metastasis of hepatocellular carcinoma. *Mod. Pathol.* **2006**, *19*, 533–540.
153. Altadill, A.; Rodriguez, M.; Gonzalez, L.O.; Junquera, S.; Corte, M.D.; Gonzalez-Dieguez, M.L.; Linares, A.; Barbon, E.; Fresno-Forcelledo, M.; Rodrigo, L.; *et al.* Liver expression of matrix metalloproteinases and their inhibitors in hepatocellular carcinoma. *Dig. Liver Dis.* **2009**, *41*, 740–748.
154. Tretiakova, M.S.; Hart, J.; Shabani-Rad, M.T.; Zhang, J.; Gao, Z. Distinction of Hepatocellular adenoma from hepatocellular carcinoma with and without cirrhosis using E-cadherin and matrix metalloproteinase. *Mod. Pathol.* **2009**, *22*, 1113–1120.
155. Gorrin Rivas, M.J.G.; Arii, S.; Furutani, M.; Harada, T.; Mizumoto, M.; Nishiyama, H.; Fujita, J.; Imamura, M. Expression of human macrophage metalloelastase gene in hepatocellular carcinoma: Correlation with angiostatin generation and its clinical significance. *Hepatology* **1998**, *28*, 986–993.
156. Nakatsukasa, H.; Ashida, K.; Higashi, T.; Ohguchi, S.; Tsuboi, S.; Hino, N.; Nouso, K.; Urabe, Y.; Kinugasa, N.; Yoshida, K.; *et al.* Cellular distribution of transcripts for tissue inhibitor of metalloproteinases 1 and 2 in human hepatocellular carcinomas. *Hepatology* **1996**, *24*, 82–88.
157. International Working Party. Terminology of nodular hepatocellular lesions. *Hepatology* **1995**, *22*, 983–993.
158. Korkaya, H.; Liu, S.; Wicha, M.S. Breast cancer stem cells, cytokine networks, and the tumor microenvironment. *J. Clin. Invest.* **2011**, *121*, 3804–3809.
159. McLean, K.; Gong, Y.; Choi, Y.; Deng, N.; Yang, K.; Bai, S.; Cabrera, L.; Keller, E.; McCauley, L.; Cho, K.R.; *et al.* Human ovarian carcinoma-associated mesenchymal stem cells regulate cancer stem cells and tumorigenesis via altered BMP production. *J. Clin. Invest.* **2011**, *121*, 3206–3219.
160. Yan, X.-L.; Jia, Y.-L.; Chen, L.; Zeng, Q.; Zhou, J.-N.; Fu, C.-J.; Chen, H.-X.; Yuan, H.-F.; Li, Z.-W.; Shi, L.; *et al.* Hepatocellular carcinoma-associated mesenchymal stem cells promote hepatocarcinoma progression: Role of the S100A4-mIR155-SOCS1-MMP-9 axis. *Hepatology* **2013**, *57*, 2274–2286.
161. Roderfeld, M.; Rath, T.; Lammert, F.; Dierkes, C.; Graf, J.; Roeb, E. Innovative immunohistochemistry identifies MMP-9 expressing macrophages at the invasive front of murine HCC. *World J. Hepatol.* **2010**, *2*, 175–179.
162. Tian, T.; Nan, K.; Guo, H.; Wang, W.; Ruan, Z.; Wang, S.; Liang, X.; Lu, C. PTEN inhibits the migration and invasion of HepG2 cells by coordinately decreasing MMP expression via the PI3K/Akt pathway. *Oncol. Rep.* **2010**, *23*, 1593–1600.
163. Park, S.Y.; Jeong, K.J.; Panupinthu, N.; Yu, S.; Lee, J.; Han, J.V.V.; Kim, J.M.; Lee, J.S.; Kang, J.; Park, C.G.; *et al.* Lysophospatidic-acid augments human hepatocellular carcinoma cell invasion through LPA1 receptor and MMP-9 expression. *Oncogene* **2011**, *30*, 1351–1359.
164. Yang, X.; Wang, D.; Dong, W.; Song, Z.; Dou, K. Inhibition of Na(+)/H(+) exchanger 1 by 5-(*N*-ethyl-*N*-isopropyl) amiloride reduces hypoxia-induced hepatocellular carcinoma invasion and motility. *Cancer Lett.* **2010**, *295*, 198–204
165. Kessenbrock, K.; Plaks, V.; Werb, Z. Matrix metalloproteinases: Regulators of the tumor microenvironment. *Cell* **2010**, *141*, 52–67.

166. Murugan, R.S.; Vinothini, G.; Hara, Y.; Nagini, S. Black tea polyphenols target matrix metalloproteinases, RECK, proangiogenic molecules and histone deacetylase in a rat hepatocarcinogenesis model. *Anticancer Res.* **2009**, *29*, 2301–2305.
167. Stefanou, N.; Papanikolaou, V.; Fukukawa, Y.; Nakamura, Y.; Tsezou, A. Leptin as a critical regulator of hepatocellular carcinoma development through modulation of human telomerase reverse transcriptase. *BMC Cancer* **2010**, *10*, 442.
168. Chen, Y.; Boyartchuk, V.; Lewis, B. Differential roles of insulin-like growth factor receptor- and insulin receptor-mediated signaling in the phenotypes of hepatocellular carcinoma cells. *Neoplasia* **2009**, *11*, 835–845.
169. Shengbing, Z.; Feng, L.J.; Bin, W.; Lingyun, G.; Aimin, H. Expression of KISS-1 gene and its role in invasion and metastasis of human hepatocellular carcinoma. *Anat. Rec. (Hoboken)* **2009**, *292*, 1128–1134.
170. Martin, D.C.; Sanchez-Swatman, O.H.; Ho, A.T.; Inderdeo, D.S.; Tsao, M.; Khokha, R. Transgenic TIMP-1 inhibits simian virus 40 T antigen-induced hepatocarcinogenesis by impairment of hepatocellular proliferation and tumor angiogenesis. *Lab. Invest.* **1999**, *79*, 225–234.

Lymph Node Stromal Cells Negatively Regulate Antigen-Specific CD4$^+$ T Cell Responses

Jun Abe,[*,†,‡] Shigeyuki Shichino,[*,†] Satoshi Ueha,[*,†] Shin-ichi Hashimoto,[*,†,§] Michio Tomura,[¶] Yutaka Inagaki,[†,‖] Jens V. Stein,[‡] and Kouji Matsushima[*,†]

Lymph node (LN) stromal cells (LNSCs) form the functional structure of LNs and play an important role in lymphocyte survival and the maintenance of immune tolerance. Despite their broad spectrum of function, little is known about LNSC responses during microbial infection. In this study, we demonstrate that LNSC subsets display distinct kinetics following vaccinia virus infection. In particular, compared with the expansion of other LNSC subsets and the total LN cell population, the expansion of fibroblastic reticular cells (FRCs) was delayed and sustained by noncirculating progenitor cells. Notably, newly generated FRCs were preferentially located in perivascular areas. Viral clearance in reactive LNs preceded the onset of FRC expansion, raising the possibility that viral infection in LNs may have a negative impact on the differentiation of FRCs. We also found that MHC class II expression was upregulated in all LNSC subsets until day 10 postinfection. Genetic ablation of radioresistant stromal cell–mediated Ag presentation resulted in slower contraction of Ag-specific CD4$^+$ T cells. We propose that activated LNSCs acquire enhanced Ag-presentation capacity, serving as an extrinsic brake system for CD4$^+$ T cell responses. Disrupted function and homeostasis of LNSCs may contribute to immune deregulation in the context of chronic viral infection, autoimmunity, and graft-versus-host disease. *The Journal of Immunology*, **2014, 193: 1636–1644.**

Lymph nodes (LNs) are the primary site of Ag encounter by lymphocytes. Circulating lymphocytes reside there for up to 24 h (1) and undergo multiple rounds of cell-to-cell contact with Ag-presenting dendritic cells (DCs) (2). The LN structure and microenvironment are designed to concentrate Ags transported from the periphery and to promote the migration and survival of lymphocytes and DCs (3–5).

LN stromal cells (LNSCs) play a critical role in the functional organization of the LNs (6). LNSCs consist of multiple types of fibroblastic cells, lymphatic endothelial cells (LECs), and blood vessel endothelial cells (BECs). One subset of fibroblastic LNSCs, fibroblastic reticular cells (FRCs) in the T cell region, produce IL-7 and exist in close contact with T cells and DCs (7, 8). FRCs also express the homeostatic chemokines CCL19/CCL21 (9–11) and ICAM-1, which together act as the guiding cue and driving force for the intranodal migration of lymphocytes and DCs (4, 12). Moreover, FRCs regulate vascular growth in reactive LNs during inflammation (13), thereby ultimately controlling lymphocyte trafficking. Therefore, FRCs represent one of the key cellular components providing structural and microenvironmental support for adaptive immune responses in LNs.

Recently, a newly described role for LNSCs as APCs in adaptive immunity has attracted much attention. In the steady-state, LNSCs differentially express peripheral tissue–specific Ags and present them to CD8$^+$ T cells for the maintenance of self-tolerance (14–16). In contrast, LNSCs stimulated with LPS for 12 h in vivo upregulate MHC class II (17). Furthermore, *Pdpn*-Cre–driven expression of a model Ag in LECs and FRCs leads to the expansion of adoptively transferred Ag-specific CD4$^+$ T cells, even under noninflammatory conditions (16). These observations suggest that the outcome of Ag presentation to CD4$^+$ T cells by LNSCs could be either immunogenic or tolerogenic, depending on the inflammatory environment. However, because previous studies used sterile models of inflammation, it remains unclear how FRCs and other LNSCs adapt functionally during replicative cytopathic virus infections.

In the current study, we performed a detailed analysis of LNSC responses during vaccinia virus (VV) infection. BECs and LECs showed rapid expansion, peaking at day 14 postinfection (p.i.). In contrast, we observed a delayed, but sustained, expansion of terminally differentiated FRCs, which were replenished by noncirculating progenitor cells in a lymphotoxin-β–dependent manner. Of note, FRCs and other LNSCs expressed MHC class II p.i., which contributed to the contraction of Ag-specific CD4$^+$ T cells at the later time points of the immune response. Taken together, our data elucidate the dynamics of LNSC expansion and function during antimicrobial immune responses.

*Department of Molecular Preventive Medicine, Graduate School of Medicine, University of Tokyo, Tokyo 113-0033, Japan; †Japan Science and Technology Agency, Tokyo 102-8666, Japan; ‡Theodor Kocher Institute, University of Bern, CH-3012 Bern, Switzerland; §Division of Nephrology, Department of Laboratory Medicine, Kanazawa University, Ishikawa 920-1192, Japan; ¶Center for Innovation in Immunoregulative Technology and Therapeutics, Graduate School of Medicine, Kyoto University, Kyoto 606-8501, Japan; and ‖Center for Matrix Biology and Medicine, Graduate School of Medicine, Institute of Medical Sciences, Tokai University, Kanagawa 259-1143, Japan

Received for publication October 31, 2013. Accepted for publication June 5, 2014.

This work was supported in part by Grant-in-Aid for Scientific Research on Priority Areas 19059004 from the Ministry of Education, Culture, Sports, Science, and Technology, Japan, the Japan Science and Technology Core Research for Evolutional Science and Technology program (to K.M.), and Grant-in-Aid for Young Scientists (B) 2379052 from the Japan Society for the Promotion of Science (to J.A.).

Address correspondence and reprint requests to Dr. Kouji Matsushima, Department of Molecular Preventive Medicine, Graduate School of Medicine, University of Tokyo, 7-3-1 Hongo, Bunkyo-ku, Tokyo 113-0033, Japan. E-mail address: koujim@m.u-tokyo.ac.jp

The online version of this article contains supplemental material.

Abbreviations used in this article: B6, C57BL/6; bm12, B6.C-H2-Ab1^{bm12}; Col1a2, type I collagen α2; DC, dendritic cell; DN, double negative; FRC, fibroblastic reticular cell; HEV, high endothelial venule; LN, lymph node; LNSC, LN stromal cell; LTβR, lymphotoxin-β receptor; LTβR-Ig, rIg Fc region–fused soluble recombinant lymphotoxin-β receptor protein; #639/#474 mice, FucciG$_1$-#639×FucciS/G$_2$/M-#474 double-transgenic mice; p.i., postinfection; popLN, popliteal lymph node; Tfh, T follicular helper; VV, vaccinia virus; VV-OVA, OVA expressing recombinant VV; WT, wild-type.

www.jimmunol.org/cgi/doi/10.4049/jimmunol.1302946

Materials and Methods

Mice, viral infection, and immunization

C57BL/6 (B6) mice were purchased from Japan SLC. *Rag2*$^{-/-}$ $OVA_{323-339}$-specific TCR-transgenic (OT-II) mice were purchased from Taconic. B6.C-H2-Ab1^{bm12} (bm12) and B6.SJL (CD45.1) mice were purchased from The Jackson Laboratory. FucciG_1-#639×FucciS/G_2/M-#474 double-transgenic mice (#639/#474 mice) on a B6 background (18) were provided by Atsushi Miyawaki (RIKEN). *Col1a2*-GFP mice were generated as described previously (19). Mice were 6–8 wk old at the commencement of experiments. Mice were either infected s.c. with 1×10^4 PFU OVA-expressing recombinant VV (VV-OVA) (20) or were hock immunized (21) with 50 μg OVA protein emulsified in CFA. In some experiments, mice were given an i.p. injection of 100 μg rIg Fc region–fused soluble recombinant lymphotoxin-β receptor (LTβR) protein (LTβR-Ig) 1 d before immunization and on a weekly basis thereafter. All animal experiments were conducted in accordance with the guidelines of the Animal Care and Use Committee of the University of Tokyo.

Abs

mAbs against CD4 (RM4-5), CD8α (53-6.7), CD11b (M1/70), CD11c (HL3), CD19 (6D5), β1 integrin (Ha2/5), CD31 (390), CD44 (IM7), CD45 (30-F11), CD45.1 (A20), CD45.2 (104), B220 (RA3-6B2), CD80 (16-10A1), CD86 (GL1), VCAM-1 (429), CD138 (281-2), CD157 (BP-3), ICOS (7E.17G9), PD-1 (RMP1-30), CXCR5 (2G8), gp38 (8.1.1), Ly-6G/C (RB6-8C5), NK1.1 (PK136), Ter-119 (TER-119), BrdU (Bu20a), MHC class I (28-14-8), I-A/I-E (M5/114.15.2), TCR Vα2 (B20.1), and TCRγδ (UC7-13D5) were purchased from BioLegend, BD Biosciences, or eBioscience and used for flow cytometry. For the immunofluorescent staining of tissue sections, purified anti–pan-endothelial Ag (MECA-32) and biotinylated anti-gp38 (8.1.1) mAbs were purchased from BioLegend, anti-type IV collagen rabbit antiserum was purchased from LSL, and Alexa Fluor–labeled secondary Abs and streptavidin were purchased from Life Technologies.

Flow cytometry

LNs were either minced by filtering through a cell strainer (BD Biosciences) or digested in 0.1% crude collagenase (Wako; cat. #32-10534), 0.96 mg/ml Dispase II (Roche), and 20 kU/ml DNase I (Calbiochem) in DMEM supplemented with 2% FCS and 10 mM HEPES for 30 min at 37°C. Throughout the digestion process, the suspension was stirred gently using a small magnetic stirrer bar. Aliquots of the resulting single-cell suspension were stained with appropriate Ab mixtures. Data were collected on a Gallios flow cytometer (Beckman Coulter) and analyzed using FlowJo software (TreeStar).

Measurement of viral load in tissues

Viral load in reactive LNs and infected footpads was measured by copy number assay. In brief, LNs and footpads were homogenized using a beads-based cell disruptor, and total DNA was isolated using a Tissue Genomic DNA Extraction Mini Kit (Favorgen). Copy numbers of *Ova* gene were measured by subjecting 45 ng total DNA/reaction to quantitative PCR with FastStart TaqMan Probe Master (Roche), a TaqMan Gene Expression Assay kit Gg03366808_m1 (for *Ova*), and a TaqMan Copy Number Reference Assay kit (Applied Biosystems). The limit of detection of the assay was 10 copies.

In vivo BrdU labeling

For short-term pulse labeling, mice were injected i.p. with 1 mg/mouse BrdU (Sigma-Aldrich) 16 h before sacrifice. For long-term continuous labeling, mice were provided with drinking water containing 0.8 mg/ml BrdU for the duration of the experiment, commencing immediately p.i. BrdU water was replaced every 2–3 d.

Immunofluorescent staining of LN sections

Six-micron-thick cryosections of fresh LNs were prepared and fixed for 10 min in acetone. Fixed sections were rehydrated with PBS, blocked with Blocking One reagent (Nacalai Tesque), and stained with Ab mixtures (in PBS containing 2% BSA) for 1 h at room temperature. Sections were incubated further with appropriate secondary Abs. For BrdU staining, sections were fixed for 10 min with 4% paraformaldehyde in PBS after the staining of the other Ags. Fixed sections were treated with 2 M HCl for 1 h at 37°C before incubation with anti-BrdU Ab. After staining, sections were mounted with ProLong Gold reagent (Life Technologies). Immunofluorescently stained sections were observed under a TCS SP5 confocal microscope (Leica Microsystems). The acquired images were processed and quantified using ImageJ software (National Institutes of Health).

Parabiosis

Parabiosis surgery was performed on body weight–matched partners. A longitudinal incision was made through the skin and fascia of mice deeply anesthetized with pentobarbital. The incised skins and fascia of partner mice were joined by sutures. More than 6 wk after the surgery, mice were infected s.c. with VV-OVA via the footpad distal to the conjoined side of the body.

Generation of bone marrow chimeric mice and adoptive transfer

CD45.1$^-$ CD45.2$^+$ bm12 and B6 recipient mice were exposed to 8.5 Gy irradiation before transplantation with 5×10^6 CD45.1$^+$ CD45.2$^+$ whole bone marrow (BM) cells the following day. More than 6 wk after transplantation, 2×10^4 CD45.1$^+$ CD45.2$^-$ *Rag2*$^{-/-}$ OT-II T cells were adoptively transferred into recipient mice via the tail vein 1 d before immunization. For OT-II T cell preparation, CD4$^+$ T cells were enriched from the spleen of OT-II mice by negative selection using streptavidin MicroBeads and an AutoMACS cell separator (Miltenyi Biotec). Before magnetic labeling with MicroBeads, cells were labeled with biotinylated Abs against CD8α, CD11b, CD11c, CD19, CD138, Ly-6G/C, NK1.1, Ter-119, and TCRγδ. The purity of CD4$^+$ TCR Vα2$^+$ OT-II T cells was routinely >95%.

Statistical analysis

Data were analyzed for statistical significance by Student *t* test (for comparison of two groups) or one-way ANOVA (for comparison of three of more groups; post hoc tests were performed as described in the figure legends). All statistical analyses were performed using GraphPad Prism software. The p values < 0.05 were considered statistically significant.

Results

LNSCs expand in a subset-specific manner during viral infection

In a recent study, immunization with protein Ag and CFA caused the number of FRCs and endothelial cells in the LNs to increase in parallel with the lymphocyte number (22). We confirmed this observation in a sterile OVA/CFA immunization model (Supplemental Fig. 1A–C). However, the expansion of LNSC subsets during antimicrobial immune responses remained to be investigated. Therefore, we developed a protocol for the flow cytometric analysis of stromal cells in reactive popliteal LNs (popLNs) following s.c. VV-OVA infection, using contralateral nonreactive popLNs as controls.

LNSCs were identified based on the differential expression of gp38 and CD31 among CD45$^-$ Ter-119$^-$ nonhematopoietic cells in the LNs (23) (Fig. 1A, Supplemental Fig. 1A). Using this approach, we observed a >10-fold increase in total popLN cell numbers, peaking on day 10 p.i. (Fig. 1B, 1C). LEC and BEC expansion peaked on day 14 p.i., with a 5-fold increase in their numbers. Strikingly, FRC expansion was significantly delayed (Fig. 1B, shaded area) but was sustained until day 28 p.i., whereas expansion of LECs and BECs began as early as day 4 p.i. (Fig. 1B, 1C). The numbers of LNSCs in the contralateral nonreactive popLNs were not affected by VV infection. The percentage of T cell region reticular cells (9) among total FRCs, identified by CD157 expression, remained essentially stable (data not shown). Of note, the onset of FRC expansion coincided with the decline of VV-OVA copy number in reactive popLNs (Fig. 1D). Viral gene was almost undetectable on day 10 p.i. in reactive popLNs, whereas virus persisted for longer at the infection site. Reactive popLNs harbored considerably less virus than the infection site throughout the time course of our analysis. Importantly, the delayed expansion of FRCs relative to that of lymphocytes and other LNSC subsets clearly demonstrates that reactive LN growth and increased FRC numbers are not synchronized in the VV-OVA infection model, unlike in sterile inflammation (22).

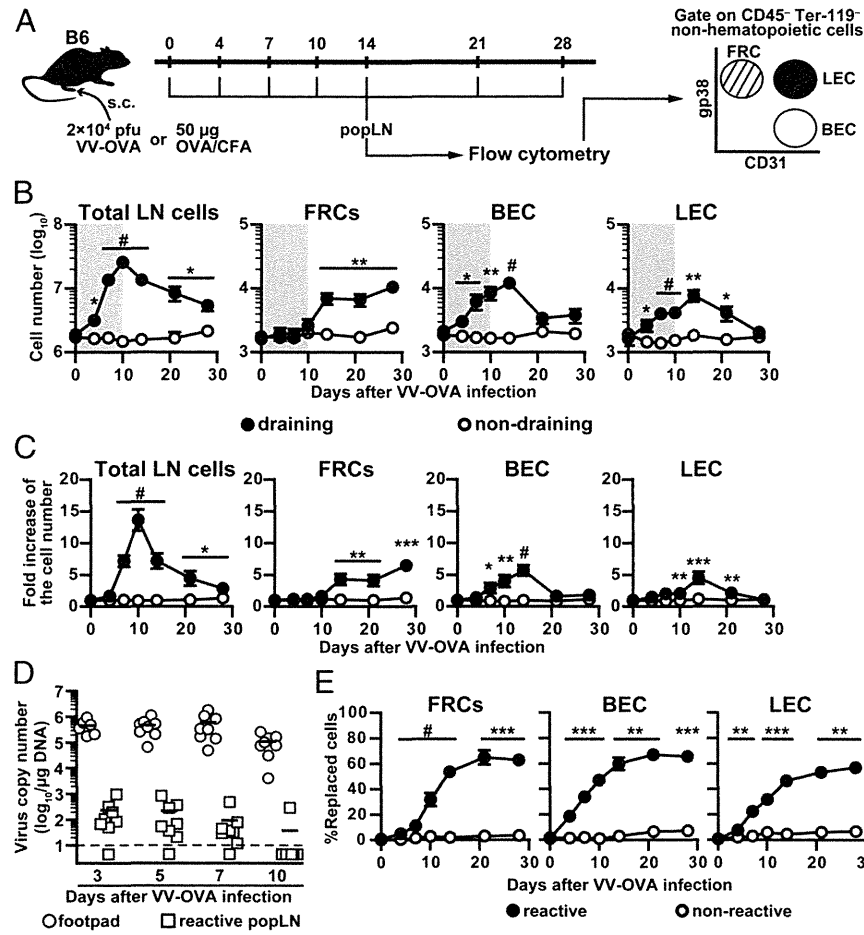

FIGURE 1. Kinetics of the FRC response following immune stimulation. (**A**) Experimental model. On day 0, mice were injected s.c. with VV-OVA or OVA/CFA via the footpad or hock, respectively. LNSC subsets in the reactive and contralateral nonreactive popLNs were analyzed by flow cytometry at various time points. Number (**B**) and fold expansion (**C**) of total LN cells, FRCs, BECs, and LECs in the reactive LNs on days 0, 4, 7, 10, 14, 21, and 28 after VV-OVA infection. Fold expansion for each subset was calculated by normalizing against mean cell number in unstimulated (day 0) popLNs. Shading in (B) indicates the time points across which FRC expansion is delayed. Graphs show the mean ± SEM of n = 17/time point, pooled from five independent experiments. (**D**) Kinetics of viral load in the infected footpads (○) and reactive popLNs (□), measured by copy number assay for the *Ova* gene. Each symbol represents one mouse (n = 8 pooled from two independent experiments), and horizontal lines indicate means. Dashed line represents the limit of detection. (**E**) Turnover of FRCs, BECs, and LECs was measured by long-term BrdU-labeling assay. Mice were provided with drinking water containing BrdU from day 0 until the time of analysis. Data represent mean ± SEM (n = 12/time point) of the proportion of BrdU$^+$ cells in reactive (filled) and contralateral nonreactive (blank) popLNs. Data are pooled from three independent experiments. $^*p < 0.05$, $^{**}p < 0.05$, $^{***}p < 0.001$, $^{\#}p < 0.0001$ versus nonreactive popLNs, Student t test.

We next investigated the turnover of LNSC subsets by continuous BrdU labeling throughout VV-OVA infection (up to day 28 p.i.). In this experimental setting, BrdU incorporation identifies cells that have been replaced within the time frame of the experiment. Turnover of endothelial cells commenced as early as day 4 p.i., whereas there was a marked increase in BrdU$^+$ FRCs from day 7 p.i. (Fig. 1E, Supplemental Fig. 1D). The proportion of BrdU$^+$ cells across all LNSC subsets remained constant after day 14 p.i., suggesting an accelerated turnover rate of these cells during the first 2 wk of acute viral infection. In nonreactive LNs, only minimal turnover of LNSCs was observed across the 28-d duration of our experiments (Fig. 1E).

Immunofluorescent staining of popLN sections revealed that FRCs were present in the central and perivascular areas of the T cell region and the medulla (Fig. 2A). FRC localization was not affected by infection. BrdU$^+$ FRCs (cells that had been replaced p.i.) were found throughout the T cell region after continuous BrdU labeling for 14 d (Fig. 2B). However, the density of BrdU$^+$ FRCs was substantially higher in the perivascular areas of both the T cell region and the medulla (Fig. 2C), suggesting that FRC precursors may be enriched in this subcompartment. Similar results were observed in mice immunized with OVA protein emulsified in CFA (data not shown).

FRCs are terminally differentiated cells that are replenished by local precursors

LNSC turnover could result from two possible events: proliferation of LNSCs themselves and/or differentiation from stromal precursor cells. We evaluated the proliferation of LNSCs after viral infection using short-term in vivo BrdU pulse-labeling experiments (Fig. 3A). Although BrdU incorporation by BECs and LECs was evident as early as day 3 p.i. and was detectable until day 14, minimal FRC proliferation was detected in reactive popLNs and only on day 7 p.i. (Fig. 3B). The low proliferation of FRCs was confirmed using #639/#474 mice, which were engineered to allow visualization of cell cycle progression in a labeling-free manner through the reciprocal expression of Cdt1-coupled Kusabira-Orange and geminin-coupled Azami-Green during the G_1 and $S/G_2/M$ phases of the cell cycle, respectively (18) (Fig. 3C). Taken together, our data suggest that FRC expansion is initiated by the generation of new FRCs by intranodal precursor cells, rather than the proliferation of terminally differentiated mature FRCs. Of note, the expansion and turnover of total CD45$^-$ CD31$^-$ gp38$^-$ double negative (DN) cells progressed with similar kinetics to those of FRCs (Supplemental Fig. 2A, 2B). Moreover, there was a readily detectable proportion of proliferating cells within the LTβR$^+$ CD31$^-$ gp38$^-$ DN LNSC population in reactive PLNs (Supplemental Fig. 2C), which could contain FRC precursor cells (11).

We also addressed whether FRCs might be replenished by circulating progenitors recruited to reactive LNs after viral infection. However, parabiosis experiments suggested that newly generated FRCs were likely derived from intranodal cells. Reactive popLNs in wild-type (WT) parabionts conjoined with type I collagen α2 (Col1a2) GFP reporter mice (19) did not contain GFP-expressing FRCs on day 14 p.i. (Supplemental Fig. 2D), when FRC turnover reached a plateau (Fig. 1E). The presence of GFP$^-$ FRCs in the reactive popLNs is consistent with a previous report

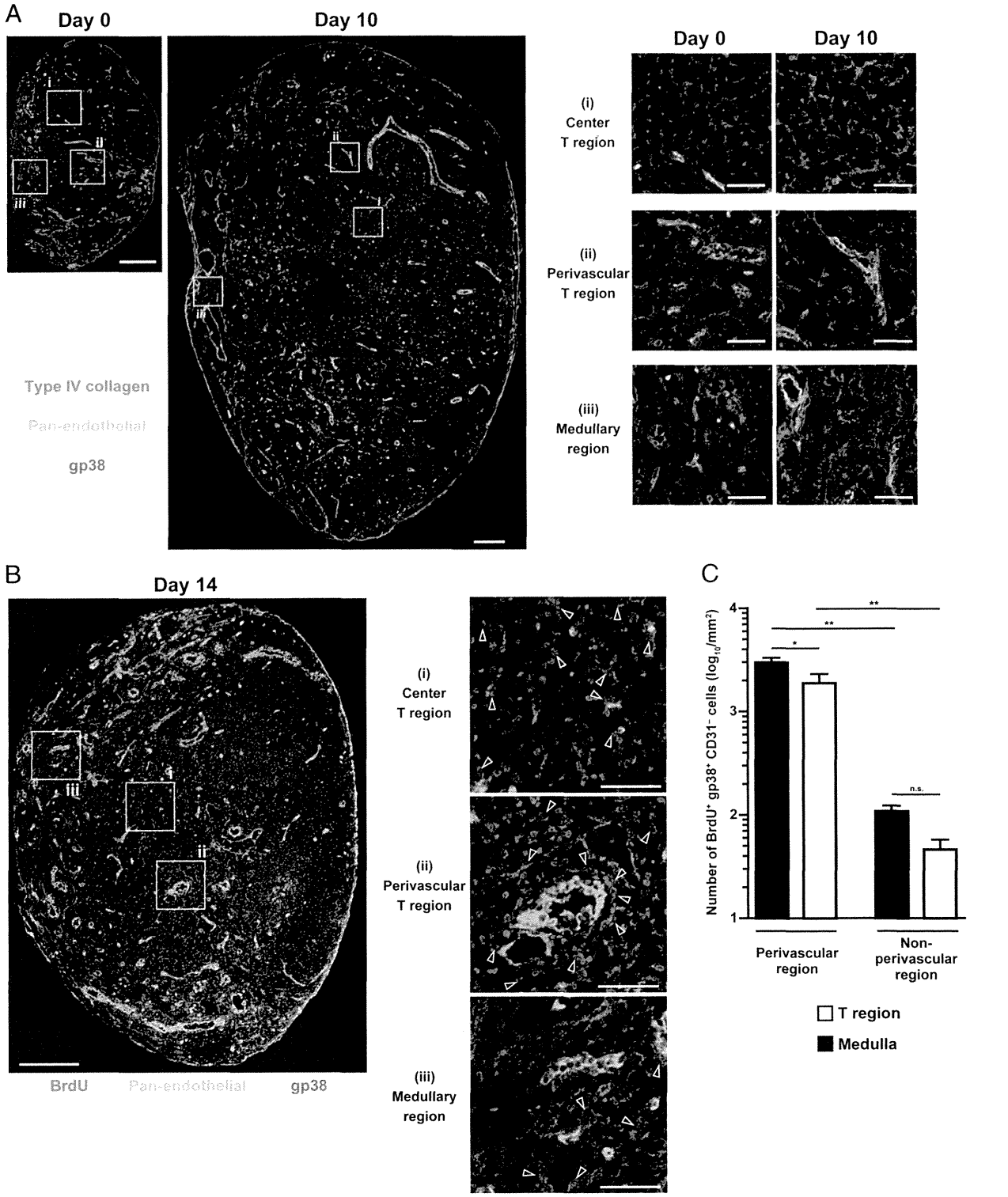

FIGURE 2. Localization of FRCs following s.c. VV-OVA infection. (**A**) Localization of FRCs in the reactive popLNs on days 0 and 10 p.i. Red, type IV collagen; green, pan-endothelial Ag; blue, gp38. Enlarged views of specific areas in the LN (*right panels*): (**i**) center of T cell region, (**ii**) perivascular area in the T cell region, and (**iii**) medulla. (**B**) Localization of $BrdU^+$ FRCs in the reactive popLNs on day 14 p.i. BrdU labeling was performed as for Fig. 1E. Enlarged views show specific areas as in (A), depicted as (**i**), (**ii**), and (**iii**). Red, BrdU; green, pan-endothelial Ag; blue, gp38. Arrowheads indicate $BrdU^+$ FRCs. Scale bars, 200 μm (*left panels*) and 50 μm (*right panels*). Representative images from six LNs are shown. (**C**) Number of $BrdU^+$ $gp38^+$ cells/mm^2 of different regions of the reactive popLNs on day 14 p.i. Three sections/LN that were ≥50 μm from each other were used for quantification. Graph shows mean ± SEM of $n = 6$ pooled from two independent experiments. $^*p < 0.05$, $^{**}p < 0.001$, one-way ANOVA with Bonferroni post hoc test. n.s., not significant.

using these reporter mice that showed that phenotypic fibroblasts in the CCl_4-treated liver also contain a GFP^- population (19). This could be due either to transcription of *Col1a2* by only a limited fraction of FRCs in a manner independent of the promoter/enhancer used in this transgenic mouse strain or to occasional epigenetic inactivation of the transgene in some FRCs.

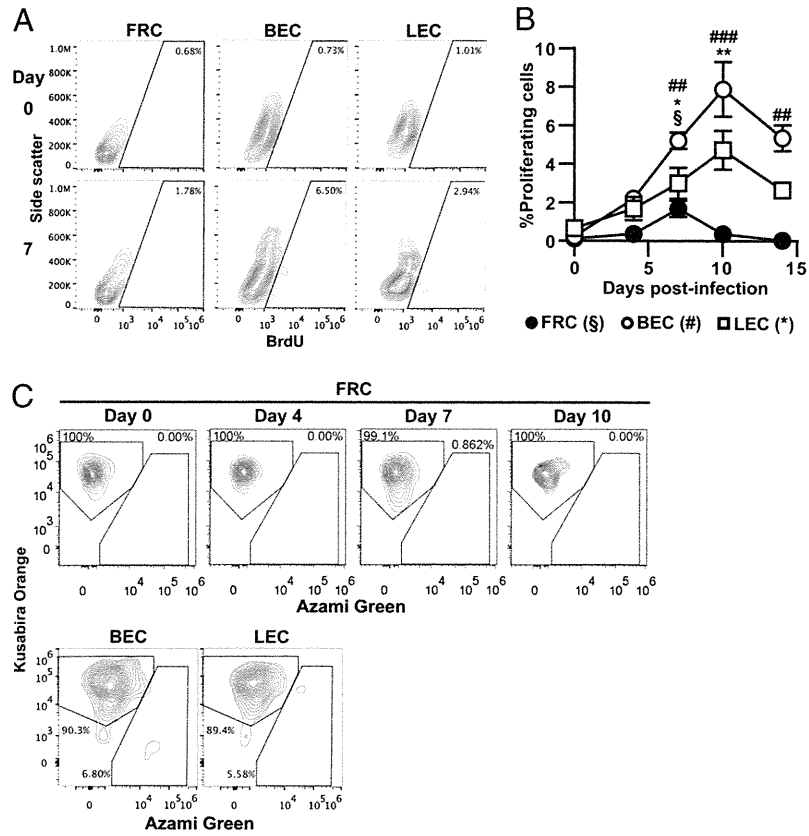

FIGURE 3. Proliferation of FRCs after viral infection. (**A** and **B**) Assessment of LNSC proliferation by short-term BrdU-labeling assay. Proliferating cells were marked by 16-h BrdU pulse labeling. Representative plots on days 0 and 7 (A) and mean ± SEM (B) of n = 12/time point pooled from three independent experiments. $^{*}p < 0.05$, $^{**,\#\#}p < 0.005$, $^{\S,***,\#\#\#}p < 0.0001$, versus day 0, one-way ANOVA with Dunnett post hoc test. The different symbols represent different comparisons as indicated below (B). (**C**) Proliferation of FRCs measured using Fucci transgenic mice. Proliferating cells were identified as Azami-Green–expressing cells. Plots gated on BECs and LECs on day 10 p.i. are shown as a positive control for Fucci-based monitoring of stromal cell proliferation. Representative plots from n = 9 pooled from three independent experiments are shown.

Lymphotoxin signaling regulates sustained LNSC subset expansion

Because LTβR plays an important role in the remodeling and maintenance of function of LNs (11, 24), we examined the involvement of LTβR-mediated signaling in FRC turnover by using the inhibitor LTβR-Ig. Unexpectedly, LTβR-Ig treatment from the time of infection reduced the number of FRCs and total LN cells in reactive popLNs only after day 14 p.i. (Fig. 4A), although FRC turnover was reduced to ~50% of that observed in control mice (Fig. 4B). Similarly, BEC, but not LEC, expansion was severely attenuated by LTβR-Ig treatment only after day 10 p.i. (Fig. 4). Notably, turnover of both FRCs and BECs ceased at earlier time points in LTβR-Ig–treated mice than in control mice. These results suggest that LTβR-mediated signaling contributes to sustained LNSC turnover but that alternative growth pathways play a more important role in the early expansion of LNSCs.

Sustained upregulation of MHC class II on LNSCs

Next, we determined whether FRCs change their activation status during viral infection. Based on flow cytometric analysis, FRCs underwent a progressive increase in cell size (forward scatter) and internal complexity (side scatter) after viral infection (Fig. 5A), indicating that FRCs remained activated from at least day 4 to day 10. β1 integrin, VCAM, CD44, platelet-derived growth factor receptors, CD80, and MHC class I were all expressed constitutively on FRCs (Fig. 5B). MHC class II surface expression levels were elevated on day 10 p.i. (Fig. 5C). Notably, the highest MHC class II expression among LNSCs was detected on CD157^{+} FRCs (Fig. 5D, 5E). This increase was observed in both BrdU^{-} and BrdU^{+} cells in long-term BrdU-incorporation experiments (data not shown).

MHC class II on LNSCs induces CD4^{+} T cell contraction after peak expansion

Based on the increased MHC class II expression detected on LNSCs, we examined the impact of stromal cell–mediated Ag presentation on CD4^{+} T cell responses, with a particular focus on the later time points of the immune response. For this purpose, lethally irradiated CD45.1^{-} CD45.2^{+} WT B6 or mutant *H2-Ab* allele–harboring bm12 mice received adoptive transfer of CD45.1^{+} CD45.2^{+} B6 BM, giving rise to B6→B6 and B6→bm12 chimera, respectively. Chimeric mice received 2 × 10^{4} H2-A^{b}–restricted CD45.1^{+} CD45.2^{-} OT-II T cells, such that the responses of monoclonal T cells with the same TCR and genetic background could be used as a functional readout. Leukocytes from different sources were discriminated using CD45 congenic markers (Fig. 6A). Remnants of recipient leukocytes accounted for 16.1 ± 1.42% and 20.2 ± 1.12% of total leukocytes in the LNs of B6→B6 and B6→bm12 chimeras, respectively. More than 90% of host-derived leukocytes were T cells (data not shown). Importantly, only 0.4 ± 0.1% and 1.3 ± 0.5% of MHC class II^{+} B cells and DCs, respectively, were of recipient origin in the LNs of B6→bm12 mice. Thus, Ag presentation to OT-II T cells in the LNs should occur under comparable conditions in both chimeras, except that LNSCs cannot present cognate peptide to OT-II cells in B6→bm12 mice because of the mutation in the *H2-Ab* gene.

Although OVA infection induced <50-fold expansion of adoptively transferred OT-II CD4^{+} T cells (data not shown), OVA/CFA immunization promoted an ~1000-fold OT-II T cell expansion in both chimeras that peaked by day 10 (Fig. 6B). Of note, we detected a substantially higher number of OT-II T cells in the reactive popLNs of B6→bm12 mice from day 21 onward (Fig. 6B), suggesting that loss of stromal cell–mediated Ag presentation leads to slower contraction of OT-II cells. In line with this observation, the number of OT-II–derived CXCR5^{+} PD-1^{hi} ICOS^{+} T follicular helper (Tfh) cells (25) was increased in B6→bm12 mice on day 21, but not day 10 (Fig. 6C), without any skewing toward Tfh cells (percentage of Tfh cells in total OT-II cells on day 21 was 18.0 ± 5.1% in WT mice and 20.9 ± 3.3% in mutant chimera, p = 0.657, Student t test). Our results demonstrate

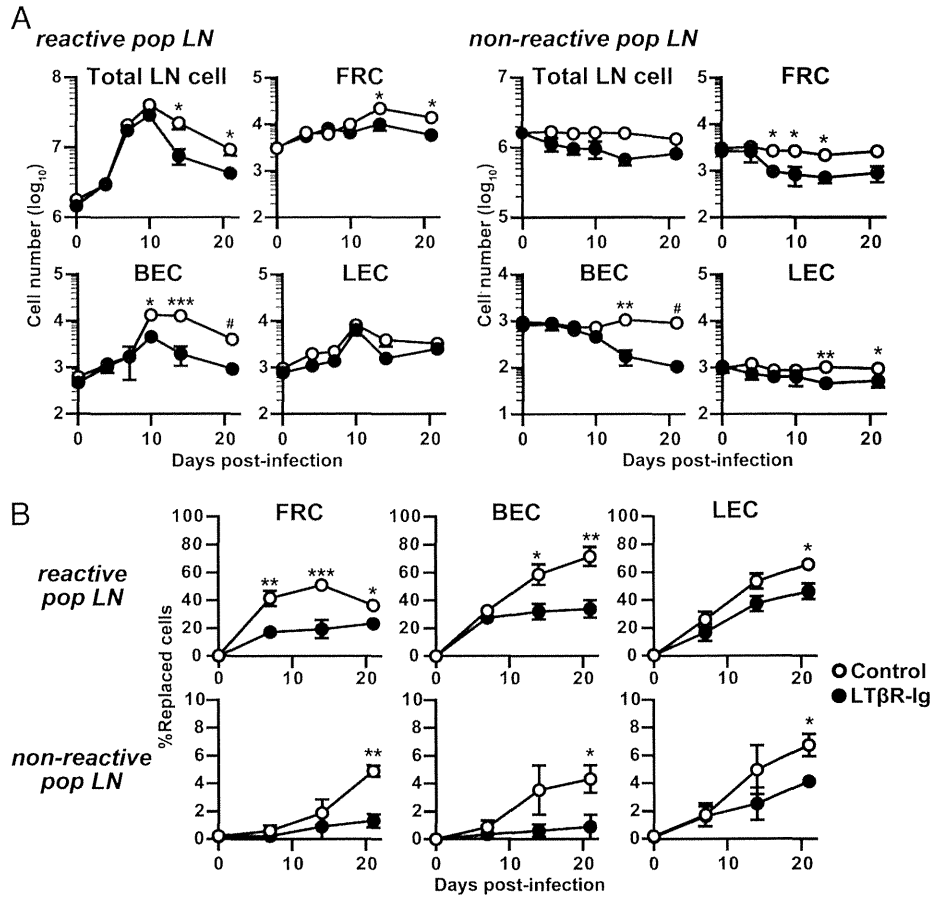

FIGURE 4. Paucity of the BEC and FRC response in the absence of LTβR-mediated signaling. Mice were injected i.p. with 100 μg LTβR-Ig once a week starting from the day before immunization. The number (**A**) and turnover (**B**) of FRCs, BECs, and LECs after VV-OVA infection were measured by flow cytometry. The results of statistical analyses comparing cell numbers against the initial number on day 0 by one-way ANOVA are summarized in Supplemental Table I. Turnover was assessed as for Fig. 1D by performing long-term BrdU-labeling assays. Graphs show the mean ± SEM of n = 9/time point pooled from three independent experiments. $^{*}p < 0.05$, $^{**}p < 0.01$, $^{***}p < 0.005$, $^{\#}p < 0.001$, reactive versus nonreactive popLNs, unpaired Student t test.

that Ag presentation by stromal cells negatively modulates the later phase of the Ag-specific $CD4^+$ T cell response.

Discussion

Although LNSCs are now recognized to play an important role in the adaptive immune response, the dynamic changes that occur in the number and function of these cells during physiologically relevant virus infection have not been investigated previously. In the current study, we used a cytopathic virus to monitor the growth and differentiation of LNSCs, with a focus on FRCs. We report a delayed, but sustained, expansion of FRCs, which was not synchronized with the expansion of other LNSC subsets or total LN cell numbers. Our data support a model in which FRCs are replenished in an LTβR-dependent manner by local precursors accumulated in the perivascular areas. At the peak of the adaptive immune response, LNSC subsets increase MHC class II expression, which contributes to $CD4^+$ T cell contraction.

Contrary to our expectation that all LNSCs would expand in parallel with incoming leukocyte numbers following viral infection, we observed substantially delayed growth of FRCs during the first week of infection. In immunofluorescent sections of reactive LNs, the FRC network on day 10 p.i. appeared more sparse compared with FRCs in control LNs. This observation may indicate the formation of a more widely spaced stromal network, either owing to mechanical stretching to accommodate increased leukocyte numbers or as a result of the death of FRCs in infected LNs. In contrast, Luther and colleagues (26) reported comparable spacing of the FRC network after immunization with a protein Ag emulsified in an adjuvant. This discrepancy may be the result of the different kinetics of FRC expansion between sterile inflammation and our viral infection models. Two weeks after viral infection, ~60% of FRCs had been replaced without substantial cellular proliferation of mature FRCs. BrdU-incorporating cells among the perivascular DN LNSC population (11) may generate new FRCs during viral infections, which is consistent with the dense accumulation of $BrdU^+$ FRCs around blood vessels that was observed in our long-term BrdU-labeling assay. The observation that increased FRC generation depends on LTβR is in line with a recent report by Ludewig and colleagues (11) showing that *Ccl19* promoter–driven conditional ablation of LTβR eliminates mature FRCs but increases the fraction of DN LNSCs. An attractive hypothesis is that high levels of lymphotoxin expression by activated lymphocytes (27) triggers the differentiation of FRCs through direct interaction with intranodal FRC precursor cells. In addition, lymphotoxin signaling may also indirectly affect FRC turnover, because LTβR blockade severely attenuated BEC expansion in LTβR-Ig–treated mice. It is noteworthy that LTβR plays an important role in remodeling (28–30) and in the functional maintenance (24) of high endothelial venules (HEVs). Long-term LTβR-Ig treatment causes a loss of HEV phenotype (24), resulting in the impaired recruitment of lymphocytes into reactive LNs during the ongoing immune response. Because our experiments extended until day 21 p.i., it is likely that HEV function was also impaired in our experiments, which, together with the attenuated BEC response, might result in the suboptimal functional adaptation of LNSCs. A potential mechanism for the attenuated LNSC response in LTβR-Ig treatment could involve, but is not limited to, a decreased amount of unidentified factors provided from recruited lymphocytes and/or BECs. In contrast, the FRC response may facilitate the BEC response, as was suggested by recent studies (13, 22), thus establishing a positive-feedback loop. Taken together, our data support a model in which FRC precursors are

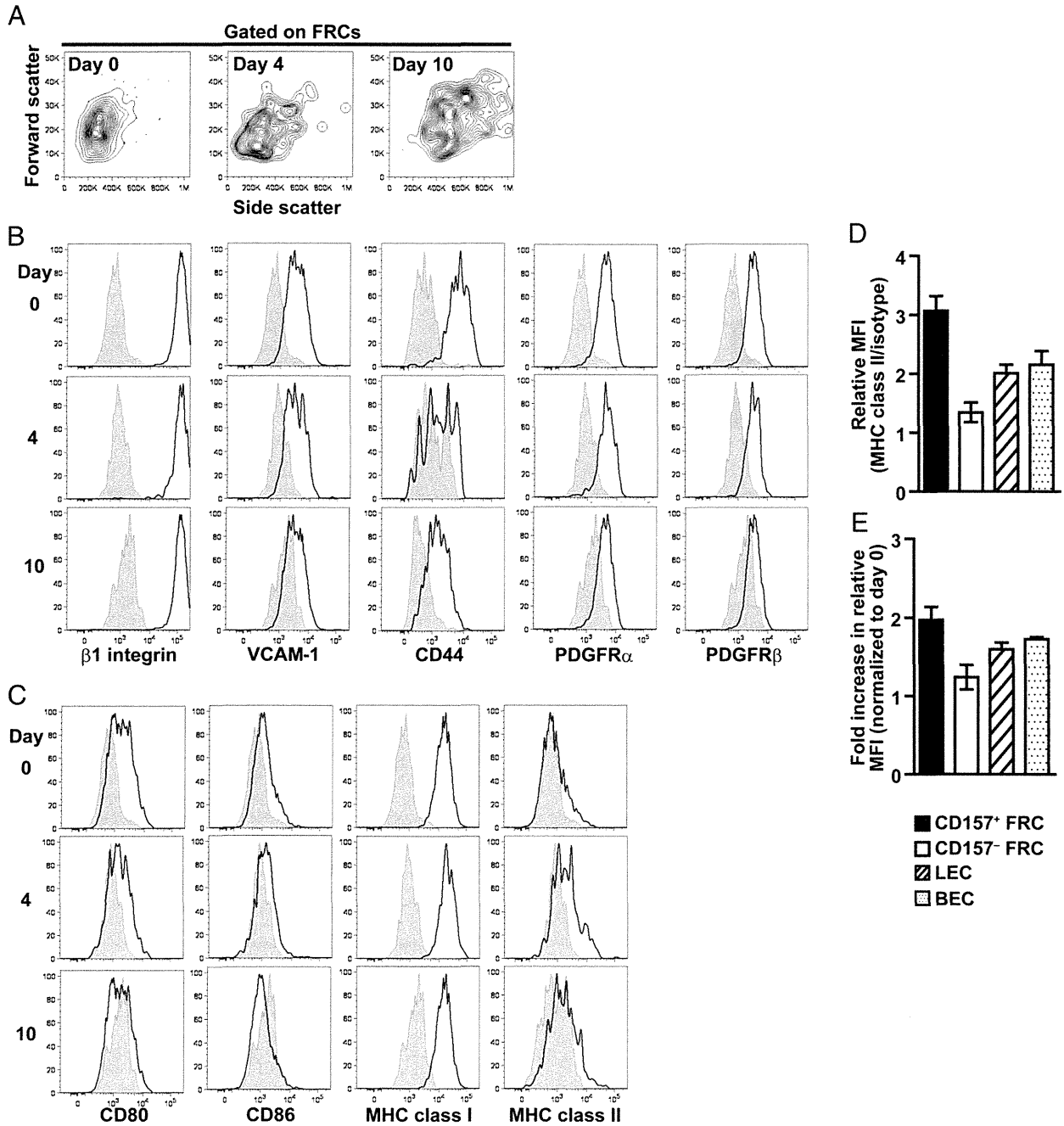

FIGURE 5. Functional changes in FRCs during viral infection. Scatter profile (**A**) and the expression of cell surface markers and MHCs (**B** and **C**) on FRCs in reactive popLNs after VV-OVA infection was analyzed by flow cytometry on days 0 (naive), 4, and 10 p.i. (**D**) Relative mean fluorescent intensity (MFI) values for MHC class II staining on day 10 p.i. Relative MFI was calculated by normalizing absolute MHC class II MFI values against MFI values for isotype-matched control staining of the same sample, to account for variations in the background intensity of each subset. (**E**) Fold increase in relative MFI of MHC class II on day 10 p.i. Representative plots (A–C) and the mean ± SEM (D and E) of $n = 9$ pooled from three independent experiments are shown.

dormant in perivascular niches. In reactive LNs, the increased influx of T and B cells, as well as other leukocytes, triggers LTβR-dependent proliferation and the gradual differentiation of the precursors into mature, nondividing FRCs. Our data also illustrate the flexibility of the adaptive immune response. Although LNSCs undergo steady growth largely parallel to leukocyte influx during sterile inflammation, cytopathic VV infections result in delayed FRC growth. However, the lymphocyte influx that is important for clonal selection is not impaired. In future studies, it will be interesting to analyze how the migratory behavior of lymphocytes changes in cytopathic VV infections.

The increased MHC class II expression by LNSCs that persisted for a long time p.i. suggests that the timing and extent of Ag presentation by LNSCs and the inflammatory microenvironment that supports Ag presentation influence the outcome of stromal Ag presentation. Possible outcomes are the maintenance of self-tolerance (31, 32), the induction of proliferation (16), or the culling of late T cell responses. In terms of the timing of Ag presentation, stromal cells in nonlymphoid tissues could also contribute to late Ag presentation to activated/effector CD4+ T cells in our BM chimera model. Although we cannot exclude this possibility, it is noteworthy that, in our experiments, total and Tfh OT-II cells were similarly

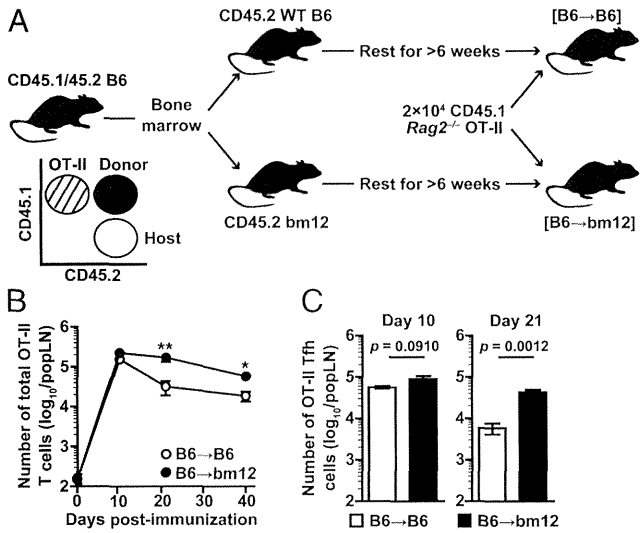

FIGURE 6. Direct Ag presentation by LNSCs curtails the CD4$^+$ T cell response. (**A**) Experimental model. Lethally irradiated CD45.1$^-$ CD45.2$^+$ WT B6 or bm12 recipient mice received 5 × 10^6 BM cells from CD45.1$^+$ CD45.2$^+$ B6 mice. More than 6 wk later, chimeric mice received 2 × 10^4 CD45.1$^+$ CD45.2$^-$ *Rag2*$^{-/-}$ OT-II cells and were immunized with OVA/CFA via the hind hock. Donor, recipient, and transgenic T cells were identified by their expression of congenic markers. (**B**) Number of total OT-II T cells in B6 (○) and bm12 (●) recipients after immunization. *p = 0.0177, **p = 0.003. (**C**) Number of OT-II T cells differentiated into CXCR5^{hi} ICOS$^+$ PD-1^{hi} Tfh cells. Statistical significance was assessed by unpaired Student t test. Graphs show the mean ± SEM of n = 7–9/time point pooled from three independent experiments.

affected by the loss of Ag presentation by stromal cells. Compared with other effector CD4$^+$ T cells, Tfh cells are long-term LN residents (33, 34) and, therefore, are less likely to encounter stromal cells in nonlymphoid tissues. Accordingly, the decreased number of Tfh cells in the absence of Ag presentation by stromal cells is likely due to the lack of Ag presentation by LNSCs. It would be worthwhile for future studies to analyze the significance of Ag presentation by stromal cells in nonlymphoid tissues, particularly in the context of tissue-resident memory T cell generation.

In conclusion, we provide novel insights into the diverse nature of LNSC responses during viral infection. We propose that LNSCs serve as an extrinsic "brake system" for late CD4$^+$ T cell responses, preventing overt responses after Ag clearance. This idea is supported, at least in part, by recent findings that the potential loss of functional FRCs in chronically SIV-infected macaques coincides with the accumulation of Tfh cells (35–37). Altered FRC functionality is also observed as decreased CCR7 ligand levels and smaller T cell regions in lupus-prone mice, which may relate to impaired immunoregulatory function (38). Furthermore, disruption of functional LN structure in graft-versus-host disease patients (39) likely involves the loss of LNSC function, which may contribute to the autoimmune-like chronic symptoms observed in this disease (40). Further studies in these different contexts will uncover the significance of this putative LNSC-mediated brake system and may lead to improved vaccination strategies or therapies for the induction of immunological tolerance.

Acknowledgments

We thank Philippa Marrack for providing VV-OVA, Atsushi Miyawaki for providing #639/#474 mice, Hiroshi Kiyono for the LTβR-Ig expression vector, Hiroyuki Yamamoto for insightful comments on the manuscript, Francis H.W. Shand for scientific editing of the manuscript, and Mizuha Kosugi-Kanaya, Ryu Takahashi, Chiaki Kasahara, Shun-ichi Fujita, Shin Aoki, Fumika Nakamura, and Ai Yamashita for excellent technical support.

Disclosures

The authors have no financial conflicts of interest.

References

1. Tomura, M., N. Yoshida, J. Tanaka, S. Karasawa, Y. Miwa, A. Miyawaki, and O. Kanagawa. 2008. Monitoring cellular movement in vivo with photoconvertible fluorescence protein "Kaede" transgenic mice. *Proc. Natl. Acad. Sci. USA* 105: 10871–10876.
2. Mempel, T. R., S. E. Henrickson, and U. H. Von Andrian. 2004. T-cell priming by dendritic cells in lymph nodes occurs in three distinct phases. *Nature* 427: 154–159.
3. Bajénoff, M., J. G. Egen, L. Y. Koo, J. P. Laugier, F. Brau, N. Glaichenhaus, and R. N. Germain. 2006. Stromal cell networks regulate lymphocyte entry, migration, and territoriality in lymph nodes. *Immunity* 25: 989–1001.
4. Schumann, K., T. Lämmermann, M. Bruckner, D. F. Legler, J. Polleux, J. P. Spatz, G. Schuler, R. Förster, M. B. Lutz, L. Sorokin, and M. Sixt. 2010. Immobilized chemokine fields and soluble chemokine gradients cooperatively shape migration patterns of dendritic cells. *Immunity* 32: 703–713.
5. Siegert, S., and S. A. Luther. 2012. Positive and negative regulation of T cell responses by fibroblastic reticular cells within paracortical regions of lymph nodes. *Front. Immunol.* 3: 285.
6. Lämmermann, T., and M. Sixt. 2008. The microanatomy of T-cell responses. *Immunol. Rev.* 221: 26–43.
7. Hara, T., S. Shitara, K. Imai, H. Miyachi, S. Kitano, H. Yao, S. Tani-ichi, and K. Ikuta. 2012. Identification of IL-7-producing cells in primary and secondary lymphoid organs using IL-7-GFP knock-in mice. *J. Immunol.* 189: 1577–1584.
8. Onder, L., P. Narang, E. Scandella, Q. Chai, M. Iolyeva, K. Hoorweg, C. Halin, E. Richie, P. Kaye, J. Westermann, et al. 2012. IL-7-producing stromal cells are critical for lymph node remodeling. *Blood* 120: 4675–4683.
9. Link, A., T. K. Vogt, S. Favre, M. R. Britschgi, H. Acha-Orbea, B. Hinz, J. G. Cyster, and S. A. Luther. 2007. Fibroblastic reticular cells in lymph nodes regulate the homeostasis of naive T cells. *Nat. Immunol.* 8: 1255–1265.
10. Scandella, E., B. Bolinger, E. Lattmann, S. Miller, S. Favre, D. R. Littman, D. Finke, S. A. Luther, T. Junt, and B. Ludewig. 2008. Restoration of lymphoid organ integrity through the interaction of lymphoid tissue-inducer cells with stroma of the T cell zone. *Nat. Immunol.* 9: 667–675.
11. Chai, Q., L. Onder, E. Scandella, C. Gil-Cruz, C. Perez-Shibayama, J. Cupovic, R. Danuser, T. Sparwasser, S. A. Luther, V. Thiel, et al. 2013. Maturation of lymph node fibroblastic reticular cells from myofibroblastic precursors is critical for antiviral immunity. *Immunity* 38: 1013–1024.
12. Woolf, E., I. Grigorova, A. Sagiv, V. Grabovsky, S. W. Feigelson, Z. Shulman, T. Hartmann, M. Sixt, J. G. Cyster, and R. Alon. 2007. Lymph node chemokines promote sustained T lymphocyte motility without triggering stable integrin adhesiveness in the absence of shear forces. *Nat. Immunol.* 8: 1076–1085.
13. Chyou, S., E. H. Ekland, A. C. Carpenter, T. C. J. Tzeng, S. Tian, M. Michaud, J. A. Madri, and T. T. Lu. 2008. Fibroblast-type reticular stromal cells regulate the lymph node vasculature. *J. Immunol.* 181: 3887–3896.
14. Fletcher, A. L., V. Lukacs-Kornek, E. D. Reynoso, S. E. Pinner, A. Bellemare-Pelletier, M. S. Curry, A. R. Collier, R. L. Boyd, and S. J. Turley. 2010. Lymph node fibroblastic reticular cells directly present peripheral tissue antigen under steady-state and inflammatory conditions. *J. Exp. Med.* 207: 689–697.
15. Cohen, J. N., C. J. Guidi, E. F. Tewalt, H. Qiao, S. J. Rouhani, A. Ruddell, A. G. Farr, K. S. Tung, and V. H. Engelhard. 2010. Lymph node-resident lymphatic endothelial cells mediate peripheral tolerance via Aire-independent direct antigen presentation. *J. Exp. Med.* 207: 681–688.
16. Onder, L., E. Scandella, Q. Chai, S. Firner, C. T. Mayer, T. Sparwasser, V. Thiel, T. Rülicke, and B. Ludewig. 2011. A novel bacterial artificial chromosome-transgenic podoplanin-cre mouse targets lymphoid organ stromal cells in vivo. *Front. Immunol.* 2: 50.
17. Malhotra, D., A. L. Fletcher, J. Astarita, V. Lukacs-Kornek, P. Tayalia, S. F. Gonzalez, K. G. Elpek, S. K. Chang, K. Knoblich, M. E. Hemler, et al.; Immunological Genome Project Consortium. 2012. Transcriptional profiling of stroma from inflamed and resting lymph nodes defines immunological hallmarks. *Nat. Immunol.* 13: 499–510.
18. Tomura, M., A. Sakaue-Sawano, Y. Mori, M. Takase-Utsugi, A. Hata, K. Ohtawa, O. Kanagawa, and A. Miyawaki. 2013. Contrasting quiescent G_0 phase with mitotic cell cycling in the mouse immune system. *PLoS ONE* 8: e73801.
19. Higashiyama, R., T. Moro, S. Nakao, K. Mikami, H. Fukumitsu, Y. Ueda, K. Ikeda, E. Adachi, G. Bou-Gharios, I. Okazaki, et al. 2009. Negligible contribution of bone marrow-derived cells to collagen production during hepatic fibrogenesis in mice. *Gastroenterology* 137: 1459–1466.e1.
20. Restifo, N. P., I. Bacík, K. R. Irvine, J. W. Yewdell, B. J. McCabe, R. W. Anderson, L. C. Eisenlohr, S. A. Rosenberg, and J. R. Bennink. 1995. Antigen processing in vivo and the elicitation of primary CTL responses. *J. Immunol.* 154: 4414–4422.
21. Kamala, T. 2007. Hock immunization: a humane alternative to mouse footpad injections. *J. Immunol. Methods* 328: 204–214.
22. Chyou, S., F. Benahmed, J. Chen, V. Kumar, S. Tian, M. Lipp, and T. T. Lu. 2011. Coordinated regulation of lymph node vascular-stromal growth first by CD11c$^+$ cells and then by T and B cells. *J. Immunol.* 187: 5558–5567.
23. Fletcher, A. L., D. Malhotra, S. E. Acton, V. Lukacs-Kornek, A. Bellemare-Pelletier, M. Curry, M. Armant, and S. J. Turley. 2011. Reproducible isolation of lymph node stromal cells reveals site-dependent differences in fibroblastic reticular cells. *Front. Immunol.* 2: 35.

24. Browning, J. L., N. Allaire, A. Ngam-Ek, E. Notidis, J. Hunt, S. Perrin, and R. A. Fava. 2005. Lymphotoxin-β receptor signaling is required for the homeostatic control of HEV differentiation and function. *Immunity* 23: 539–550.
25. Crotty, S. 2011. Follicular helper CD4 T cells (TFH). *Annu. Rev. Immunol.* 29: 621–663.
26. Yang, C. Y., T. K. Vogt, S. Favre, L. Scarpellino, H. Y. Huang, F. Tacchini-Cottier, and S. A. Luther. 2014. Trapping of naive lymphocytes triggers rapid growth and remodeling of the fibroblast network in reactive murine lymph nodes. *Proc. Natl. Acad. Sci. USA* 111: E109–E118.
27. Browning, J. L., I. D. Sizing, P. Lawton, P. R. Bourdon, P. D. Rennert, G. R. Majeau, C. M. Ambrose, C. Hession, K. Miatkowski, D. A. Griffiths, et al. 1997. Characterization of lymphotoxin-α β complexes on the surface of mouse lymphocytes. *J. Immunol.* 159: 3288–3298.
28. Webster, B., E. H. Ekland, L. M. Agle, S. Chyou, R. Ruggieri, and T. T. Lu. 2006. Regulation of lymph node vascular growth by dendritic cells. *J. Exp. Med.* 203: 1903–1913.
29. Kumar, V., E. Scandella, R. Danuser, L. Onder, M. Nitschké, Y. Fukui, C. Halin, B. Ludewig, and J. V. Stein. 2010. Global lymphoid tissue remodeling during a viral infection is orchestrated by a B cell-lymphotoxin-dependent pathway. *Blood* 115: 4725–4733.
30. Kumar, V., S. Chyou, J. V. Stein, and T. T. Lu. 2012. Optical projection tomography reveals dynamics of HEV growth after immunization with protein plus CFA and features shared with HEVs in acute autoinflammatory lymphadenopathy. *Front. Immunol.* 3: 282.
31. Lukacs-Kornek, V., and S. J. Turley. 2011. Self-antigen presentation by dendritic cells and lymphoid stroma and its implications for autoimmunity. *Curr. Opin. Immunol.* 23: 138–145.
32. Fletcher, A. L., D. Malhotra, and S. J. Turley. 2011. Lymph node stroma broaden the peripheral tolerance paradigm. *Trends Immunol.* 32: 12–18.
33. Fazilleau, N., M. D. Eisenbraun, L. Malherbe, J. N. Ebright, R. R. Pogue-Caley, L. J. McHeyzer-Williams, and M. G. McHeyzer-Williams. 2007. Lymphoid reservoirs of antigen-specific memory T helper cells. *Nat. Immunol.* 8: 753–761.
34. Fazilleau, N., L. J. McHeyzer-Williams, H. Rosen, and M. G. McHeyzer-Williams. 2009. The function of follicular helper T cells is regulated by the strength of T cell antigen receptor binding. *Nat. Immunol.* 10: 375–384.
35. Zeng, M., A. J. Smith, S. W. Wietgrefe, P. J. Southern, T. W. Schacker, C. S. Reilly, J. D. Estes, G. F. Burton, G. Silvestri, J. D. Lifson, et al. 2011. Cumulative mechanisms of lymphoid tissue fibrosis and T cell depletion in HIV-1 and SIV infections. *J. Clin. Invest.* 121: 998–1008.
36. Petrovas, C., T. Yamamoto, M. Y. Gerner, K. L. Boswell, K. Wloka, E. C. Smith, D. R. Ambrozak, N. G. Sandler, K. J. Timmer, X. Sun, et al. 2012. CD4 T follicular helper cell dynamics during SIV infection. *J. Clin. Invest.* 122: 3281–3294.
37. Lindqvist, M., J. van Lunzen, D. Z. Soghoian, B. D. Kuhl, S. Ranasinghe, G. Kranias, M. D. Flanders, S. Cutler, N. Yudanin, M. I. Muller, et al. 2012. Expansion of HIV-specific T follicular helper cells in chronic HIV infection. *J. Clin. Invest.* 122: 3271–3280.
38. Abe, J., S. Ueha, J. Suzuki, Y. Tokano, K. Matsushima, and S. Ishikawa. 2008. Increased Foxp3(+) CD4(+) regulatory T cells with intact suppressive activity but altered cellular localization in murine lupus. *Am. J. Pathol.* 173: 1682–1692.
39. Horny, H. P., H. A. Horst, G. Ehninger, and E. Kaiserling. 1988. Lymph node morphology after allogeneic bone marrow transplantation for chronic myeloid leukemia: a histological and immunohistological study focusing on the phenotype of the recovering lymphoid cells. *Blut* 57: 31–40.
40. Tyndall, A., and F. Dazzi. 2008. Chronic GVHD as an autoimmune disease. *Best Pract. Res. Clin. Haematol.* 21: 281–289.

supplemental Table 1 Statistical analysis of Fig.4 cell counts as compared to day 0

Group	Days p.i.	Reactive popLNs				Non-reactive popLNs			
		Total	FRC	BEC	LEC	Total	FRC	BEC	LEC
Control	4	n.s.	n.s.	n.s.	n.s.	n.s.	n.s.	n.s.	n.s.
	7	< 0.001	n.s.	n.s.	n.s.	n.s.	n.s.	n.s.	n.s.
	10	< 0.001	n.s.	< 0.001	< 0.001	n.s.	n.s.	n.s.	n.s.
	14	< 0.001	< 0.001	< 0.001	n.s.	n.s.	n.s.	n.s.	n.s.
	21	n.s.	< 0.005	n.s.	n.s.	n.s.	n.s.	n.s.	n.s.
LTβR-Ig	4	n.s.	n.s.	n.s.	n.s.	n.s.	n.s.	n.s.	n.s.
	7	< 0.001	< 0.05	n.s.	n.s.	n.s.	n.s.	n.s.	n.s.
	10	< 0.001	< 0.05	< 0.005	< 0.001	n.s.	< 0.05	n.s.	n.s.
	14	< 0.05	< 0.005	n.s.	n.s.	< 0.05	< 0.05	< 0.05	n.s.
	21	n.s.	n.s.	n.s.	n.s.	< 0.05	< 0.05	< 0.001	n.s.

Cell numbers at each time point were compared with those on day 0 by one-way ANOVA with Dunnett's post-hoc test.

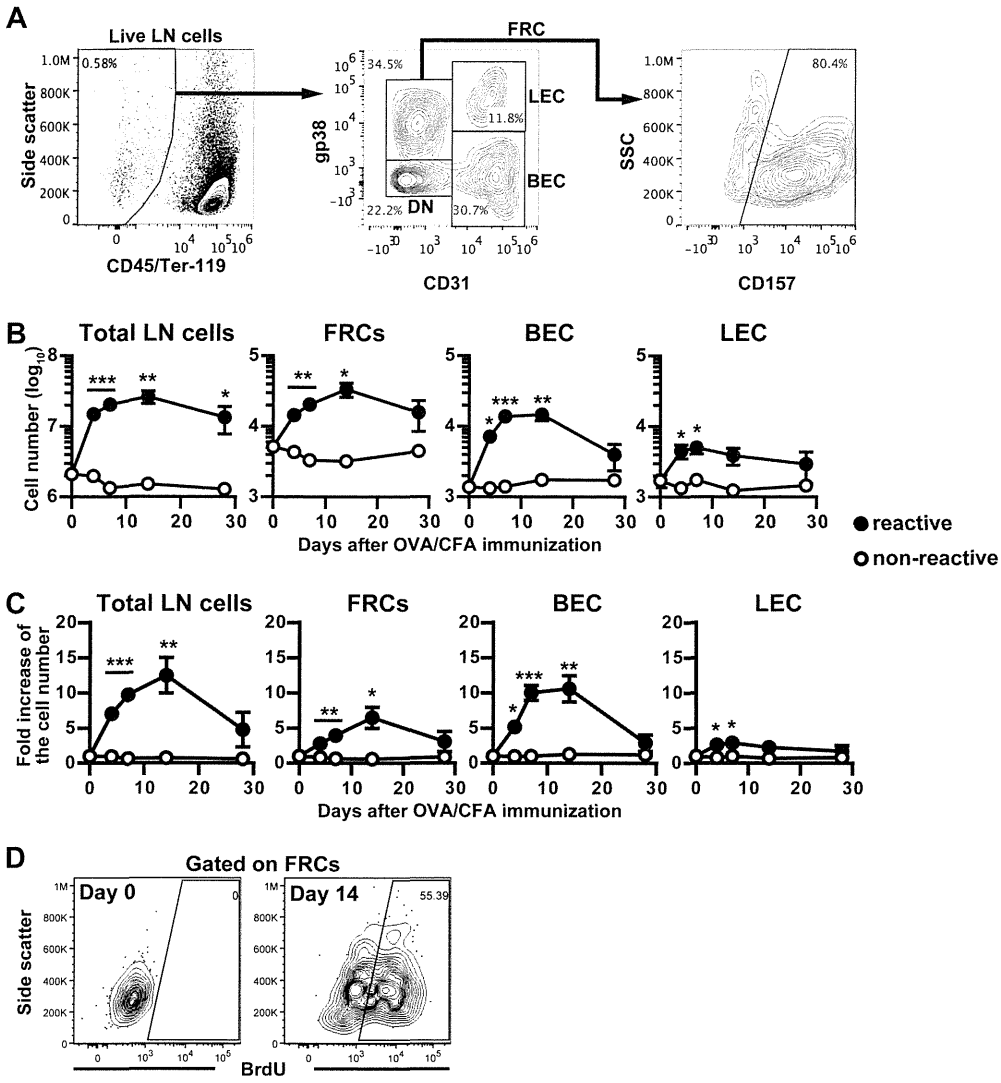

Supplemental Figure 1. Kinetics of LNSC response after OVA/CFA immunization. (A) Gating scheme for the identification of LNSC subsets. Plots from a naive popLN are shown. (B–C) Kinetics of the number (B) and fold-increase (C) of total LN cells, FRCs, BECs and LECs in reactive and contralateral non-reactive popLNs after OVA/CFA immunization. Mice were treated and analyzed as shown in Fig.1A, but immunized with OVA/CFA instead of VV-OVA.Number of LNSCs were assessed on day 0, 4, 7, 14, and 28.Graphs show the mean ± SEM of n = 9 per time point pooled from three independent experiments. $^{*}p < 0.05$, $^{**}p < 0.005$, $^{***}p < 0.001$ by Student' s *t*-test. (D) Flow cytometry of BrdU incorporation by FRCs on day 0 and day 14 p.i. by VV-OVA in long-term BrdU labeling experiments. Representative plots of n = 12 for each time point pooled from three independent experiments are shown.

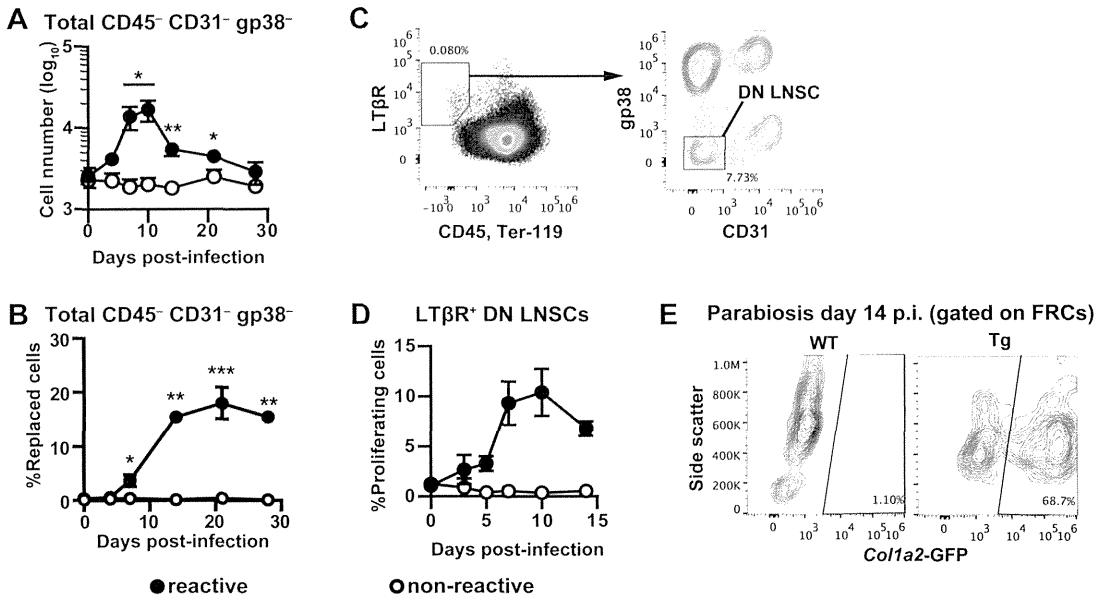

Supplemental Figure 2. Possible contribution of DN LNSCs to FRC turnover. (A) Kinetics of the number of DN cells in reactive popLNs after subcutaneous VV-OVA infection. Graph shows the mean ± SEM of n = 17 per time point pooled from five independent experiments. (B) Turnover of CD45⁻ CD31⁻ gp38⁻ cells in reactive LNs during VV-OVA infection. Graph shows the mean ± SEM of n = 9 per time point pooled from three independent experiments. (C–D) Identification of DN LNSCs (C) and kinetics of the frequency of proliferating LTβR⁺ DN LNSCs (D). Proliferation was measured by 16 hr BrdU pulse labeling. Graph shows the mean ± SEM of n = 7 per time point pooled from two independent experiments. (E) Contribution of blood-borne cells to FRC turnover analyzed by parabiosis between Col1a2-GFP transgenic and wild type mice. Each parabiont was infected with VV-OVA more than 6 weeks after surgery. Prevalence of GFP expressing FRCs in reactive PLNs was monitored by flow cytometry on day 14 post-infection. Note that WT LN is devoid of GFP⁺ cells. Representative data of n = 6 pooled from two independent experiments are shown. *$p < 0.05$, **$p < 0.001$, ***$p < 0.0001$ by Students t-test compared with non-draining popLN.

シンポジウム

3. 臓器の線維化とその治療
1）肝臓の線維化とその治療

稲垣　豊　住吉　秀明

Key words：Liver fibrosis, Fibrogenesis, Fibrolysis, Fibrosis marker

はじめに

肝線維症は，肝炎ウイルスの持続感染やアルコールの過剰摂取，非アルコール性脂肪肝炎(Non-alcoholic steatohepatitis：NASH)の他にも，自己免疫学的機序，肝内胆汁うっ滞，薬剤性，金属代謝異常，うっ血肝など，様々な原因により引き起こされる共通の病態である．線維化進展に伴って，肝組織中にはコラーゲンをはじめとする細胞外マトリックスが過剰に沈着し，その終末像である肝硬変では肝細胞機能不全や門脈圧亢進症が進行する．さらに，高頻度に合併する肝細胞癌の発生を抑止するうえでも，肝線維化機序の解明と治療法の開発は喫緊の研究テーマである．肝線維化の過程における星細胞の活性化機序や，線維組織中に増加するコラーゲンとその分解酵素の産生調節機構など，肝線維化研究は近年大きな進歩を遂げた．

しかしながら，臨床の現場に目を向けると，今もって肝線維症に対する特異的かつ効果的な治療薬は存在しない．培養細胞を用いた試験や動物実験によって多くの抗線維化作用物質が同定・報告されていながら，なぜ臨床で充分な効果を発揮できないのであろうか．本稿では，肝線維症の可逆性や肝線維症治療が従前にも増して重要視されている背景を概説するとともに，新たな治療薬の開発と臨床応用に向けて克服すべき問題と今後の展望について論じたい．

1．肝線維化は可逆的な病態である

肝線維化研究の先達であるPérez-TamayoやRojkindらが臨床例における肝硬変の可逆性を指摘して以来，すでに半世紀近くが経過した．当初はヘモクロマトーシスやWilson病といった代謝性疾患の報告が多かったが，その後のウイルス性肝炎に対する治療法の進歩は，その原因の如何を問わずに肝線維化の改善が起こりうることを証明した．アルコール性肝硬変の禁酒症例

東海大学医学部再生医療科学，東海大学大学院医学研究科マトリックス医学生物学センター

111th Scientific Meeting of the Japanese Society of Internal Medicine: Symposium: 3. Fibrosis of the viscera and its treatment; 1) Reversibility and treatment of liver fibrosis.

Yutaka Inagaki and Hideaki Sumiyoshi : Department of Regenerative Medicine, School of Medicine, Tokai University, Japan and Center for Matrix Biology and Medicine, Graduate School of Medicine, Tokai University, Japan.

本講演は，平成26年4月13日（日）東京都・東京国際フォーラムにて行われた．